Supplemental Material to the article "Modeling the quantum Hall effect in samples with longwave weak disorder"

This additional material includes: method for calculating potential $U(x, y)$; dependences of DoS(E), conductance G, and 2DEG density n at Fermi level E_F; LDoS and current J in some potential $U(x, y)$ with a long-wave disorder. Dependences of density n are shown in the absence of disorder (ideal case). Numbers of cited publications [4, 10, 14, 15, 19, 27, 28, 33], and Figures 1–4 relate to the main article. Figures from this additional material are referred to as S1–S5.

Potential $U(x, y)$ was found by numerical Thomas–Fermi method solution of a 3D electrostatic problem for a fixed distribution of localized charges in a plane remote from 2DEG. The distribution was found by the Monte-Carlo method under the following assumptions. It is an equilibrium distribution for a fixed number of localized charges frozen at a certain temperature. In the equilibrium the charges are allowed to move continuously within an ideal plane. The system of the localized charges together with their image charges in the closely placed gate is electrically neutral and does not feel 2DEG far away. The method for calculating localized charge distribution was described in [33].

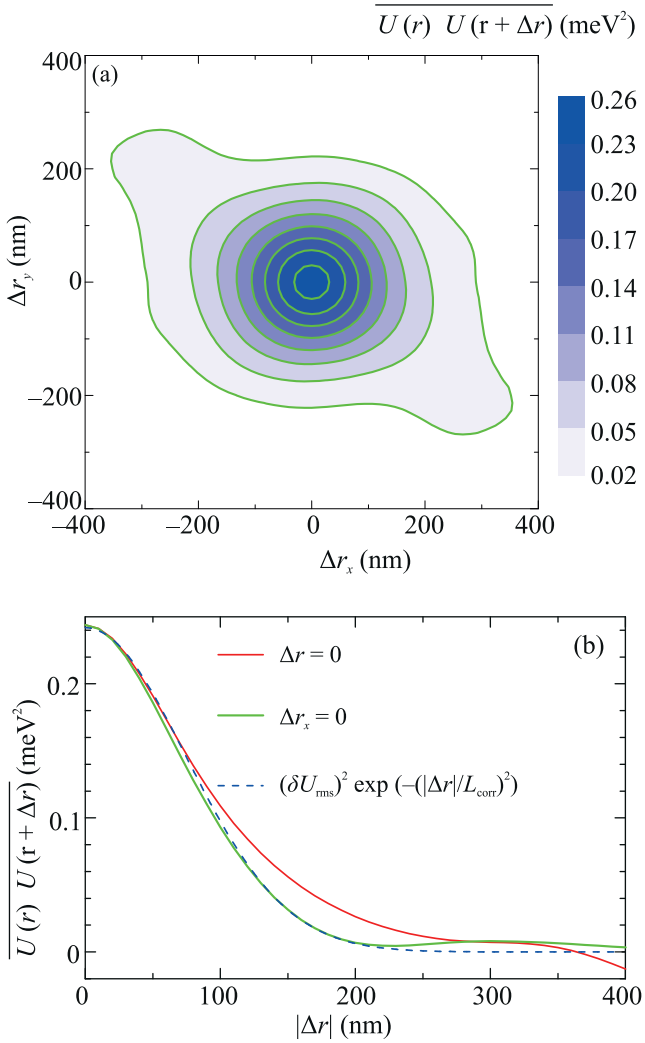

Fig. S1. Correlator of potential (a), and its cross sections along the axes $\Delta \mathbf{r}_y = 0$, $\Delta \mathbf{r}_x = 0$ together with the fitting curve at $L_{\mathrm{corr}} = 105\,\mathrm{nm}$ (b), for one of the realizations of $U(x, y)$ on a $2 \times 2\,\mu\mathrm{m}^2$ square

The interaction of these charges and image charges in the gate provided a correlated distribution at about 1000 K disorder freeze temperature. This value was determined by comparing computed transport and quantum scattering times in 2DEG to experimental data. It represents an upper boundary for actual freezing temperature, because the proposed method ignores any disorder factors except temperature. However, the calculated structural factor $F(q)$, characterizing the distribution of localized charges, was 3 times lower than that for perfectly random distribution, at small wave numbers q [33].

Statistical properties of the long-wave disorder are numerically found as correlator $\overline{U(\mathbf{r})U(\mathbf{r}+\Delta\mathbf{r})}$ for arbitrary individual implementation of $U(x,y)$. This means averaging over $\mathbf{r}$ and determining the correlation length $L_{\rm corr}$ for approximating the correlator by $(\delta U_{\rm rms})^2\exp(-|\Delta\mathbf{r}|^2/L_{\rm corr}^2)$ with $L_{\rm corr}^2 \equiv \overline{|\Delta\mathbf{r}|^2}$.

An example of the correlation function for one of the implementations $U(x,y)$ on a square of size $2{\times}2\,\mu$m^2 is shown in Fif. S1. The anisotropy in Fig. S1 is due to the unique distribution of the localized charges in the particular state of the sample. Increasing the size of the sample or averaging over the implementations of $U(x,y)$ suppresses the anisotropy.

The amplitude of the disorder was controlled by multiplying the calculated potential $U(x,y)$ by some factor A, whereas the potential in the connected channels was defined by constant $-\Delta U$. Then the problem of quantum electron scattering was solved in the whole region (Fig. 1 in the main work).

Conductance G, local density of states $\mathrm{LDoS}(x,y)$ and computational domain-average $\mathrm{DoS}(E) \equiv \overline{\mathrm{LDoS}(E)}$ were calculated by the method of nonequilibrium Green functions [27, 28] for given magnetic field and electron energy E. The definition of the Green's function includes a small imaginary addition of $i\gamma$ to the energy, which determines the level broadening. To calculate the fine structure in the Landau band, the value of γ must be less than the average distance between energy levels. The main part of the calculations was performed with small value of $\gamma < 10^{-5}$ meV. But for averaging over the spectrum it is enough to take $\gamma = 0.01$ meV.

Calculated energy dependences are shown in Fig. S2a, b for the potential, which is shown in Fig. 4c in the main work. Tall narrow spikes of $\mathrm{DoS}(E)$ of width $\Gamma \sim \delta U_{\rm rms}$ correspond to Landau bands (Fig. S2a). They are spaced by wide areas of low density of states associated with edge states. Shoulder-like features of DoS develop to the left of each Landau band at a distance of ΔU. This means that the connected channels are filled before the scattering region becomes open for transmission. Agreement is not bad between the shown dependence of $\mathrm{DoS}(E)$ and the measured $\mathrm{DoS}(E-E_F)$ in a high mobility 2DEG at $B = 2$ T and even filling factors ν [19].

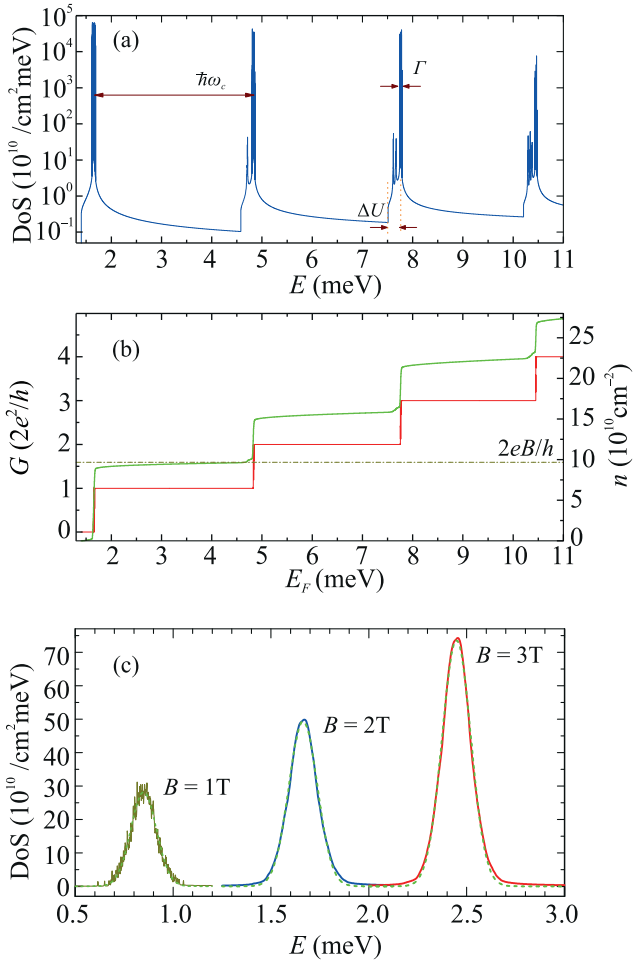

Fig. S2. (a), (b) – $\mathrm{DoS}(E)$, $G(E_F)$ and $n(E_F)$ dependences calculated at $B = 2$ T, $\gamma = 5\cdot10^{-6}$ meV for potential $U(x,y)$ given on the square $1{\times}1\,\mu$m^2 with $L_{\rm corr} \approx 80$ nm, $\delta U_{\rm rms} = 0.016$ meV and $\Delta U = 0.25$ meV (same as for Fig. 2 in the main work). (c) – $\mathrm{DoS}(E)$ calculated for potential given on the square $2{\times}2\,\mu$m^2 with $L_{\rm corr} \approx 105$ nm (same as in Fig. S1), $\delta U_{\rm rms} = 0.07$ meV, $\Delta U = 0$ for $B = 1$ T and $\gamma = 10^{-3}$ meV; and for $B = 2$ T, $B = 3$ T for $\gamma = 10^{-2}$ meV. Gaussian approximations are shown with dotted lines

Individual peaks merge into a total splash of width $\Gamma \sim \delta U_{\rm rms}$, i.e. they become indistinguishable on Fig. S2a, unlike that of Fig. 2. The calculated conductance $G(E_F)$ and 2DEG density $n(E_F)$ are shown in Fig. S2b, where one can see very sharp conductance quantization steps with the width of plateaus equal to the cyclotron gap $\hbar\omega_c$. The decrease in the cyclotron gap occurs due to insufficiently small grid cell size ($h_x = h_y = 10\,$nm). Halving the cell size ($h_x = h_y = 5\,$nm) fixes the situation, but qualitatively the results do not change.

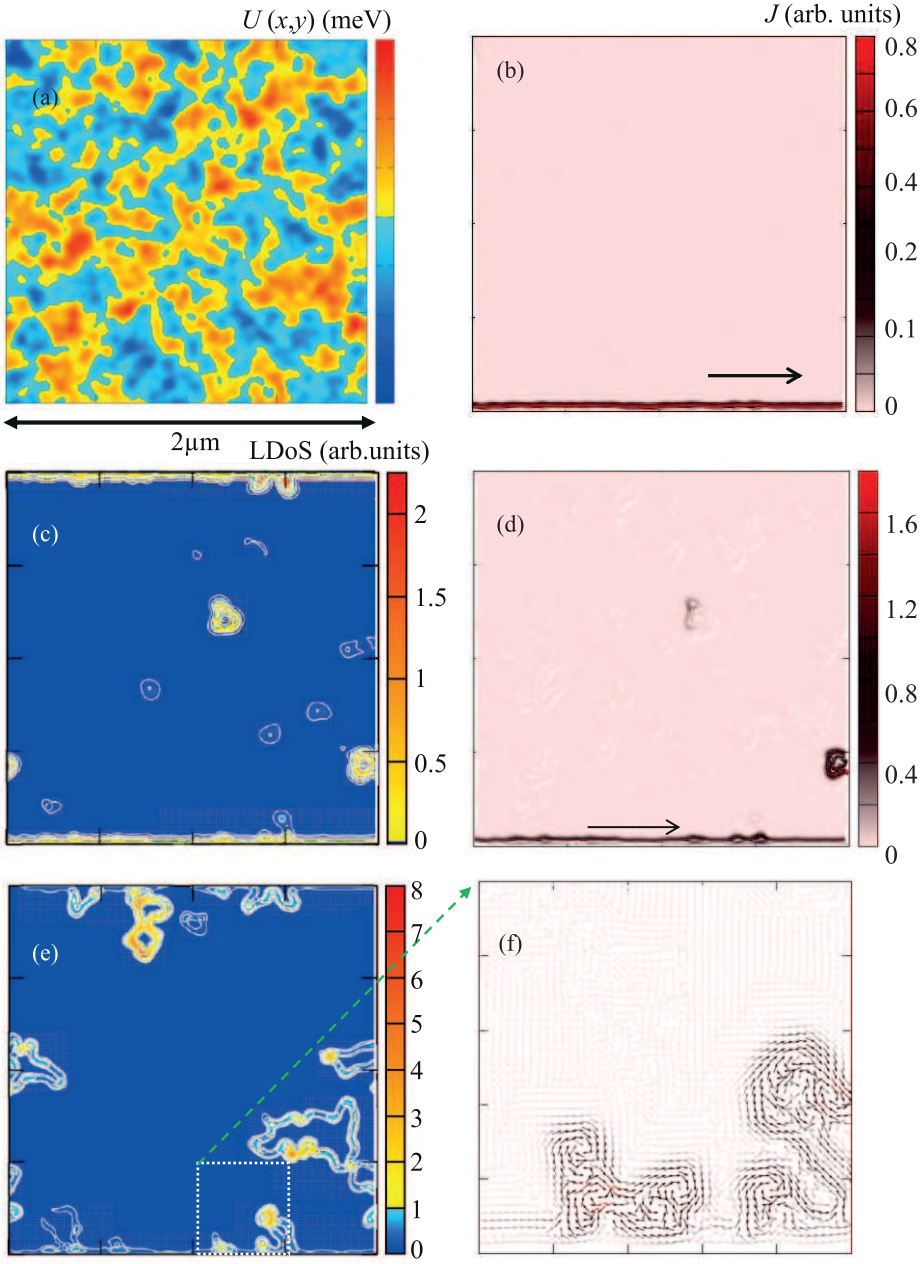

Fig. S3. (a) – $U(x, y)$ for long-wave disorder with $L_{\rm corr} \approx 80\,$nm (same as the main work), but substantially larger scattering area and $\delta U_{\rm rms}$. (b) – An example of the density of nonequilibrium current for a state near the center of the quantum plateau $G = 2e^2/h$: $E_F = \hbar\omega_c = 3.46\,$meV. (c), (d), (e), (f) – Examples of LDoS(x, y) and $J(x, y)$ for states far from the center of the same plateau: $G = 2e^2/h$ at $E_F = 2.46\,$meV and $E_F = 2.1\,$meV

Figure S2c shows the spectrum-averaged DoS(E) dependences for the lower Landau band for the disordered potential ($\delta U_{\rm rms} = 0.07\,$meV) given on the square $2 \times 2\,\mu$m^2 and different magnetic fields $B = 1$, 2, and 3 T. Landau bands have become much wider than in Fig. S2a due to almost 5× increase in the strength of the disorder. The left curve in Fig. S2c was calculated for $B = 1\,$T, $\gamma = 10^{-3}\,$meV, and oscillations in the density of states are still visible. The curves for $B = 2$ and 3 T were calculated for $\gamma = 10^{-2}\,$meV. Smooth dependencies DoS(E) with graphical precision are matched by the Gaussians, and only distribution tails go slightly higher. Note that increasing the parameter γ leads to averaging of DoS(E) over the spectrum. With this increase the area under the curve, which determines the

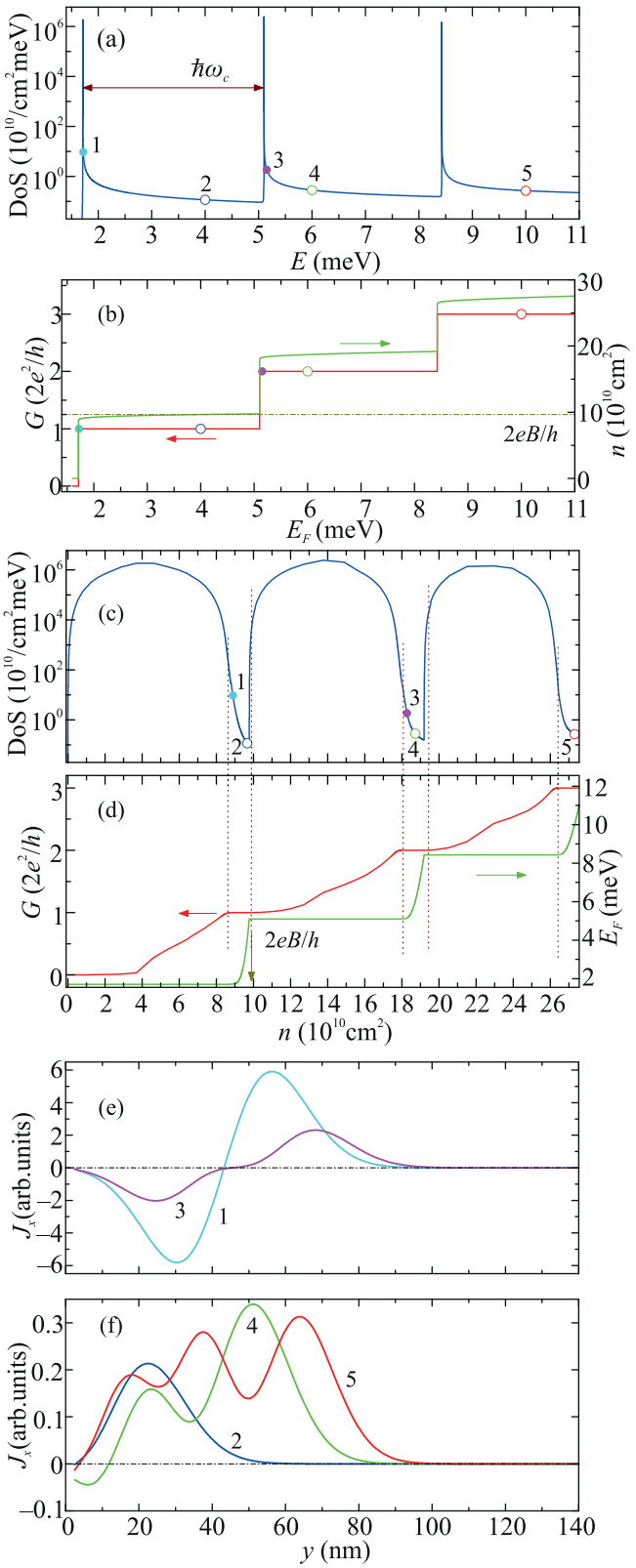

Fig. S4. (a), (b) – DoS(E), $G(E_F)$ and $n(E_F)$ dependences calculated for an ideal scatterer in a 1 μm wide channel. (c), (d) – Dependences of DoS(n), $G(n)$ and $E_F(n)$ for this case. Vertical dotted lines correspond to the edges of quantized plateaus of conductance. (e), (f) – Dependences $J_x(y)$ for the states indicated by respective dots in (a)–(c)

total population of the Landau level, is preserved, and the general course of the $n(E_F)$ dependencies remains almost unchanged. The widths of all three curves in Fig. S2c are almost equal to $2 \cdot \delta U_{\rm rms}$. They are independent of B and the number of Landau level, as it should be for a long-wave disorder in 2DEG [4]. Thus, the form DoS(E) for the Landau bands at large value of broadening parameter γ in small systems turns out to be the same as in analytical calculations

for macroscopic two-dimensional of systems [14, 15]. Calculated $U(x, y)$, LDoS(x, y) and nonequilibrium current $J(x, y)$ for channel width $2\,\mu$m and smooth disorder with $\delta U_{\rm rms} = 0.5$ meV is shown in Fig. S3. It is interesting to compare it with the main work, where the scattering area was 4 times smaller and the disorder was 30 times weaker. The case of the normal edge state with unidirectional nonequilibrium current is shown in Fig. S3b with $E_F = \hbar\omega_c = 3.46$ meV and $G = 2e^2/h$. The cases where the edge current and small current rings coexist at substantially smaller $E_F = 2.46$ meV and $E_F = 2.1$ meV are shown by LDoS in Fig. S3c, e. These energies correspond to localized states (narrow peaks of DoS). Note that similar patterns of small LDoS rings were observed experimentally in [10]. The calculated currents in Fig. S3d, f flow along the lines of constant $U(x, y) = E_F - \hbar\omega_c/2$ and do not affect the edge current that provide strict conductance value $G = 2e^2/h$, even if the individual rings of LDoS happen to be in close contact with the edge current, as shown in Fig. S3e, f. These figures and other calculations in addition to Fig. 2 of the main work show that the effect of the penetration of strict plateaus of conductance into the tails of Landau bands is fairly common. We note without illustration that with these parameters of the potential and for $1.6 < E_F < 1.8$ meV the same bidirectional current along isolines of $U(x, y)$ is observed as in Fig. 4 of the main work.

We also calculated DoS(E), $G(E_F)$ and $n(E_F)$ for $B = 2$ T in the absence of disorder $U(x, y) = 0$, $\Delta U = 0$ for channel width $1\,\mu$m. This ideal case is shown in Fig. S4a, b for comparison with the case of disorder in Fig. S2a, b. The width and height of ultra-thin DoS peaks are determined only by the imaginary additive $i\gamma$. The gaps between spikes of DoS(E) correspond to the usual edge states in a multimode channel in a perpendicular magnetic field. The energy dependences are similar to those with weak disorder (Fig. S2), except for the details. By analogy with Fig. 2 from the main work, Figures S4c, d show the same values as the function of the 2DEG density. Narrow peaks of DoS(E) turned into wide humps of DoS(n), and, accordingly, the gaps $\hbar\omega_c$ look narrow on n dependences. The behavior of dependences in Fig. 2 and Fig. S4c, d are different. For example, without disorder the widths of conductance plateaus are much narrower than transition regions between them. The situation is reversed in the case of weak disorder (Fig. 2). However, the microscopic picture of the edge states is similar in the two cases. So, nonequilibrium current flows only along the lower part of the channel: the longitudinal component $J_x(y) = 0$ for $y > 100$ nm (Fig. S4e, f). The numbers near the curves $J_x(y)$ correspond to the states with integer conductance values $G_0 = 2e^2/h$ that are shown by dots with the same numbers and color on Fig. S4a–c. Figure S4e corresponds to the states at the lower edges of the first and second conductance plateaus, i.e. low electron drift velocity. Sign change of $J_x(y)$ at $y < 100$ nm means counter currents at the lower edge of the channel. Figure S4f shows normal edge states of unidirectional nonequilibrium current corresponding to high electron drift velocities.

Finally, Fig. S5 shows the sensitivity of the quantum Hall effect to the width of the channel (ideal case). It can be seen that the dips in DoS caused by the edge states become narrow sharply with increasing this width from 1 to $3\,\mu$m. Simultaneously, the width of strict quantum plateau in units of 10^{10} cm^{-2} decreases from 0.8 down to 0.2. The widths of the DoS dips and the conductance plateaus are approximately the same.

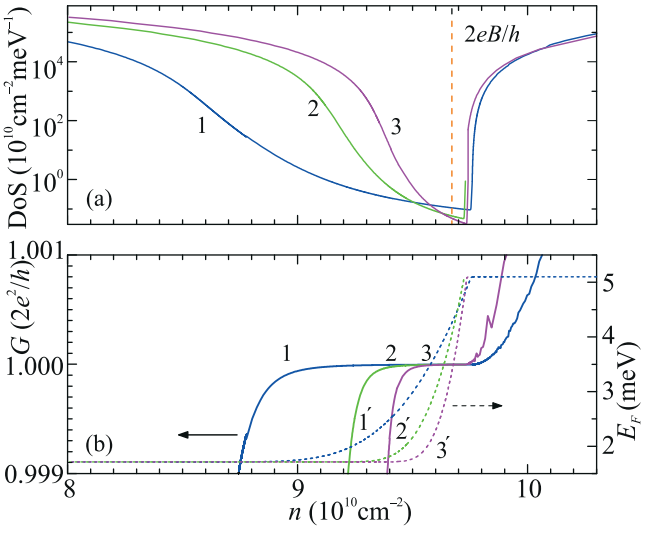

Fig. S5. Dependences DoS(n) (a), $G(n)$ and $E_F(n)$ (b) in a small range of n near the lower plateau of conductance, calculated for clean channels of width 1, 2, and $3\,\mu$m for $B = 2$ T. Colors of the corresponding solid lines DoS(n), $G(n)$ and dashed lines $E_F(n)$ are the same, the numbers near these curves indicate the channel width in μm

The contribution of the area of edge states to the total area of the sample tends to zero with increase of the sample size. The corresponding dips in DoS shrink. Thus, we can expect the contraction of the plateau of conductance to a point, i.e. *in the absence of disorder* the quantum Hall effect should be destroyed in any large samples. According to the proposed model, the situation is radically changing in the presence of weak long-wave fluctuations of $U(x, y)$

in the samples. This disorder plays an important role in the experimental observation of quantum Hall effect in the most perfect semiconductor structures (see References in the main work).